ORIGINAL RESEARCH

Negative impact of constant RPM control strategy on ship NOx emission in waves

Mohammad Hossein Ghaemi[1] · Hamid Zeraatgar[2]

Abstract
In severe wave conditions, the ship propulsion system is loaded with high fluctuations due to external disturbances. The highly fluctuating loads enforce radical changes in the main engine torque, which in turn demands variation of the fuel rate injected into the cylinders if a constant rotational speed strategy is applied. Therefore, the temperature of gases varies to a large extent during the combustion process in the cylinders. The emitted NOx is a function of this highly fluctuating temperature. The main goal of this study is to investigate NOx emission under the aforementioned conditions when a usual constant RPM control strategy is applied in waves similar to the calm water condition. The paper presents a mathematical model of the whole system, which is applied to a selected ship both in regular waves and in calm water conditions. The results show that the sea waves, in comparison with the calm water condition, can radically increase the emitted NOx under the constant rotational speed strategy. This change can reach even 10^{14} times more, averagely. The results also show that the higher the wave height the higher the emitted NOx. It is concluded that the control strategy of keeping the engine rotational speed in waves at a constant level is the most important reason for the significantly increased NOx emission in waves in comparison with the calm water condition.

Abbreviations

CII	Carbon intensity indicator
ECA	Emission control areas
EEDI	Energy Efficiency Design Index
EEXI	Energy Efficiency of Existing Ship Index
EGR	Exhaust gas recirculation
EIAPP	Engine International Air Pollution Prevention
GHG	Greenhouse gases
HC	Unburned hydrocarbons
IVMD	Instantaneous-value multidimensional model
IVZD	Instantaneous-value zero-dimensional model
HCCI	Homogeneous charge compression ignition
NMVOC	Non-methane volatile organic compounds
MVZD	Mean-value zero-dimension model
PAH	Polycyclic aromatic hydrocarbons
PM	Particular matter
SCR	Selective catalytic reduction
TWCEL	Total weighted cycle emission limit

Letters

a	Added (due to wave)
A	Area, equivalent area, advance
c	Specific heat coefficient
C	Coefficient
D	Diameter
E	Engine
h	Propeller immersion height
J	Moment of inertia, number
k	Coefficient, wave number
K	Coefficient
m	Mass, model
M	Torque (moment)
n	Rate of revolution
p	Pressure
pw	Orbital inflow
P	Power
q	Heat calorific value
Q	Torque

✉ Mohammad Hossein Ghaemi
ghaemi@pg.edu.pl

1. Faculty of Mechanical Engineering and Ship Technology, Institute of Ocean Engineering and Ship Technology, Gdańsk University of Technology, G. Narutowicza 11/12, 80-233 Gdańsk, Poland

2. Department of Maritime Engineering, Amirkabir University of Technology, Tehran, Iran

R	Gas constant, resistance, radius
t	Thrust deduction factor, time, total (due to wave)
T	Temperature, total, thrust
u	Velocity in the x-direction ($\bar{u}$: amplitude)
V	Volume
w	Wake fraction coefficient
x	Longitudinal axis, surge (added mass)
y	Transverse axis
z	Vertical axis
Z	Number of cylinders

Greek letters

β	Diminution factor
Δ	Overall ship mass
ζ	Wave profile function
η	Efficiency, coordinate
κ	Adiabatic exponent
λ	Coefficient, the ratio of ship length to model length
μ	Heading angle
π	Pressure ratio
ρ	Density
φ	Phase angle
ψ	Flow function
ω	Angular velocity

Lower indexes

0	Ambient condition
1	Point before compressor, x-direction
2	Point after compressor, y-direction
3	Point after charge air cooler (before cylinders), z-direction
4	Point after cylinders, roll (angle)
5	Point after the turbine, pitch (angle)
6	Yaw (angle)
am	Air intake manifold (receiver)
at	Atmosphere
b	Burnt (fuel)
C	Compressor
clr	Charge air cooler
comb	Combustion
cr.	Critical
cyl	Engine cylinders
e	Encounter
E	Engine
f	Fuel
gr	Exhaust gas receiver
loss	Energy/power/torque losses
n	Net
p	(At constant) pressure, prismatic
P	Propeller
T	Turbine
TC	Turbocharger

v	(At constant) volume
w	Cooling water

Upper index

*	Equivalent

Introduction

Higher efficiency, large availability, reliability, high power capacity, and easier maintenance are some of the advantages of diesel engines. That is why they are still considered as the main prime movers of ships [1]. They are being also utilized as auxiliary engines for electricity generation on shipboards. Simultaneously, they emit a relatively high amount of greenhouse gases (GHGs) due to the type of fuel they consume, and their characteristics. The main GHGs that diesel engines emit are NOx, SOx, COx, PM, and HC, among which CO and NO are the most toxic and harmful gases [2]. The emission of NOx from fossil fuels dominantly increases tropospheric ozone and hydroxyl-radical concentrations over their natural 'background' levels, thereby increasing the oxidizing power of the atmosphere [3]. Recent advances in studying air quality and the health effects of shipping emissions are discussed by Contini and Merico [4].

Reduction of emission of GHG in shipping has been one of the main goals of the International Maritime Organisation (IMO) with adopting an amendment to the MARPOL Chapter VI, providing mandatory Energy Efficiency Design Index (EEDI). Additionally, IMO currently proposed applying the Energy Efficiency of Existing Ships Index (EEXI) and Carbon Intensity Indicator (CII). These measures impose radical change on the maritime industry. Based on Annex VI, Regulations 13.8 and 5.32, starting from 2000, the Engine International Air Pollution Prevention (EIAPP) certificate is required for all ships that are equipped with marine diesel engines over 130-kW output power independent of the ship's tonnage [5]. This mainly addresses the level of NOx emission and is put in order by defining three levels (Tiers) depending on the year of building and the rate of shaft revolution. All new buildings after January 1, 2016, must satisfy the criterion of Tier III. This limitation is related to those ships that are operating in the emission control areas (ECAs). Bouman has presented a comprehensive review of the technologies, measures, and potential for reducing GHG emissions from shipping taking into account 150 up-to-date research studies [6].

Regarding the above requirements, many technological solutions during the last two decades have been provided, which can be divided into two parts: primary and secondary. The main primary methods are decrease in injection duration, delay of the start of injection and pre-injection, modification of fuel injectors, controlling the combustion

pressure, increasing the ability and efficiency of scavenging air cooler, Miller cycle, water injection, and exhaust gas recirculation (EGR) [7, 8]. There are several secondary methods, while selective catalytic reduction (SCR) method is the most well-accepted solution, today [9]. There are many studies in which different solutions, methods, and strategies are compared to each other, e.g. [9–11].

Additionally, the possibility of using different fuels and their impact has been included in other studies. As an example, Jeevahan et al. have shown that although biodiesel produces higher NOx emissions with slightly lower brake thermal efficiency and advantages of reduced emissions of CO2, CO, HC, and smoke, there are some strategies such as fuel treatments, low-temperature combustion, mixing fuel additives and reformulating fuel composition that leads to the reduction of NOx emission [12].

Research on the reduction of NOx increased starting in 1970, and the fundamental keys were mathematical models (both analytical and numerical), intensive experimental tests and measurements, and related simulations. Cakir presented a combustion model to account for the nitric oxide formation in diesel engines and compared the analytical model results with experimental data [13]. Way introduced methods for calculating the exhaust gas compositions and determining the NOx amount [14]. Miller described the mechanism and modelling of nitrogen chemistry in the combustion process [15].

Correa measured NOx emissions for a 250-MW-class combined-cycle unit for power generation with gaseous fuel and concluded that NO is formed in a distributed zone manner when the equilibrium and super-equilibrium effects can broaden the NOx-forming zones beyond the fine scales of turbulence, even in non-premixed flames [16]. Additionally, the experimental results showed that the pressure and the structure of the turbulent flow field have a diminishing effect on NOx emissions in progressively leaner premixed combustion [16]. Chikahisa et al. investigated the process of NO formation and its characteristics in diesel engines using different emission control ideas and showed that the NO formation rate is independent of the mixing of combustion gas [17]. The most important result of this study was identifying that NO emission is roughly proportional to the inverse of engine speed. Kikuta et al. analysed combustion and NO formation in large diesel engines using scale model experiments and compared them with the theoretical predictions [18]. Particularly, the study describes flow patterns and flame distribution leading to determining the heat release rates and thermal efficiency. Then, based on these identifications, an algorithm to predict NO emissions was suggested.

Rausen et al. introduced several empirical formulae for identifying the combustion duration and heat release for a homogeneous charge compression ignition (HCCI) using a mean-value model [19]. Merker provided integrated information on the simulation of combustion and pollutant formation for engine development [20]. Aspiron presented combined physics-based equations and empirical formula, which takes engine speed, injected fuel mass, the cylinder charge, its composition, and the start of combustion with the corresponding pressure and temperature as inputs and calculates the NOx emission [21]. Arregle et al. showed that the accuracy of the in-cylinder air mass and the in-cylinder total mass is much more critical than that of the instantaneous in-cylinder pressure and the injected fuel mass for NOx prediction [22]. Therefore, accurate modelling of the intake air and EGR mixture temperature and fresh air mass is crucial to be able to rationally predict the NOx emission.

Egnell presented a multi-zone combustion diagnostic method, where measured pressure data were used to calculate the heat release, local temperatures and concentrations of NO and other species [23]. Lamaris et al. also employed a multi-zone combustion model to estimate the performance characteristics and the NOx emissions of a 12.5-MW large-scale two-stroke diesel engine [24]. Mocerino et al. developed a model using Ricardo WAVE software to simulate the dynamics and emissions of an internal combustion engine [25]. The model was employed as a tool for the evaluation of emissions, particularly NO. Papagiannakis [26], Benvenuto [27] and Stoumpos [28] analysed the emission characteristics of dual-fuel engines. Scappin et al. introduced and utilized a zero-dimensional two-zone combustion model to simulate the performance and NOx emissions of a low-speed marine diesel engine using the extended Zeldovich mechanism [29]. They achieved an accuracy of 95% in comparison with a full-scale experiment. In the context of multi-zone models, Hountalas, Savva and Raptotasios studies are also important [30–32].

Hybrid propulsion solutions and their impact on emissions have also reached the great attention of scholars [33]. Last but not least, it should be mentioned that the accurate measurement of the gas composition has also assisted to improve the models and better setting up their parameters [34, 35].

The goal of this study is the evaluation of the consumed fuel and emitted NOx as one of the most harmful components of GHG in sea waves in comparison with calm water. To define the problem, it should be noted that ships are mostly navigating in sea waves rather than in the calm water. A ship and its propulsion system in the calm water are in the steady condition, whereas, in sea waves, their performances are dominated by wave oscillations. In these circumstances, engine torque and speed fluctuate in response to the ship's motion, which in turn enforce the engine's subsystems' performances to behave oscillatory. The above literature review reveals that the problem of GHG emission in sea waves has not been addressed by them. Therefore, the investigation of NOx as one of the main elements of GHG in sea waves

under the control strategy of constant engine speed (as usual practice) seems to be necessary, and it is the main objective of this study. This problem is related to several areas of research such as ship motion, propeller hydrodynamic performances in waves, engine, and subsystem performances in waves. On that basis, the simplification for the modelling of whole systems is inevitable. Here, to study the impact of sea waves on the ship emissions, when the engine is equipped with a conventional speed governor, first a mathematical model is developed in which the dynamic of the hull, propeller and engine in wave conditions is combined with the control strategy of the constant rotational speed of the engine. The mathematical model allows us to evaluate the consumed fuel as well as NOx as an important part of GHG. In the second stage of the study, a computer code is developed in MATLAB-SIMULINK for simulation purposes. Thirdly, this model is simulated for a selected ship in two regular waves and compared to the calm water conditions. In the fourth stage, a comparative analysis is conducted, where the system performances for calm and wave conditions are compared. The results show a radical increase of NOx in waves in comparison with the calm water when the same control strategy is applied in all conditions. The new elements and contribution of the results of the study in the related research field include describing the impact of the traditional control strategy of constant rotational speed for ships on the fuel consumption and NOx emission profile in wave conditions, as well as explaining the changing of ship NOx emission of a ship in response to the sea wave.

Methodology and modelling

Generally, to evaluate the consumed fuel and the emitted GHG of ships in waves, several dynamic systems have to be coupled. They include hull motion in waves, propeller performance in waves, diesel engine behaviour under the selected control strategy to control the fuel rate, as well as engine subsystems. Having the mathematical model, then its parameters should be selected and set up. This can be done based on the model and experimental test or manufacturers' data. Here, the results of model tests have been used both for ship hull resistance and for propeller open water characteristics. The engine parameters have been set using the manufacturer's data. Next, the model is coded for simulation. The simulations are conducted for two regular sea head waves and in the related calm water under three different ship speeds. The results of simulation in the time domain that include the variables of the coupled system are then used to evaluate the impact of waves and constant rotational speed control strategy on the NOx emission. The developed mathematical model enables determining the average NO emission.

In this section, a justification for the selected type of mathematical model of the engine has been presented, firstly. Then, a description of the subsystems is provided, and finally, the mathematical models of each subsystem are delivered.

Selecting the type of engine model

The diesel engine performances in unsteady states are usually analysed using four model types.

Engine model type A set of simple first- or second-order transfer functions, which determine output variables, mainly engine torque, average indicated pressure, or temperature, in response to the input variables (fuel rack or fuel rate) as a black box.

Engine model type 2 Mean-Value Zero-Dimension (MVZD) model in which the mean value of variables such as mass flow rate, temperature, and the fuel-to-air ratio is determined for each block of diesel engine (for example including compressor, turbine, manifolds, charge air cooler, etc.), while all cylinders are considered as a single block.

Engine model type 3 Instantaneous-Value Zero-Dimensional (IVZD) model, in comparison with MVZD, all variables are calculated instantaneously and individually for each cylinder.

Engine model type 4 Instantaneous-Value Multidimensional (IVMD) model that is similar to IVZD, while the output variables are additionally determined depending on the geometric coordinates.

IVZD and IVMD models can be one-zone or multi-zone, and single-phase or multi-phase flow models, particularly with respect to the combustion process. Generally, IVZD or IVMD models with two-phase flow consideration including pure air and air mixed with exhaust gases are able to simulate the instantaneous unsteady values of NOx formation. However, the MVZD model evaluates the NOx emission as a function of averaged temperature along a cycle, which is less than the real combustion temperature, for which the NOx emission should be calculated for a period of combustion. This approach has one significant weakness, which is assuming a linear distribution of NOx emission over time. The assumption, to some extent, disregards the strong nonlinearity of NOx formation as a function of combustion temperature. Since the present study aims to compare the NOx emission under different operation conditions in sea waves with respect to calm water, applying an MVZD model seems to be justified when simultaneously reducing the time and cost of simulation.

The subsystems

To achieve the goal of the study, it is necessary to develop the mathematical model of the following subsystems: (1)

Fig. 1 The layout of the mathematical model
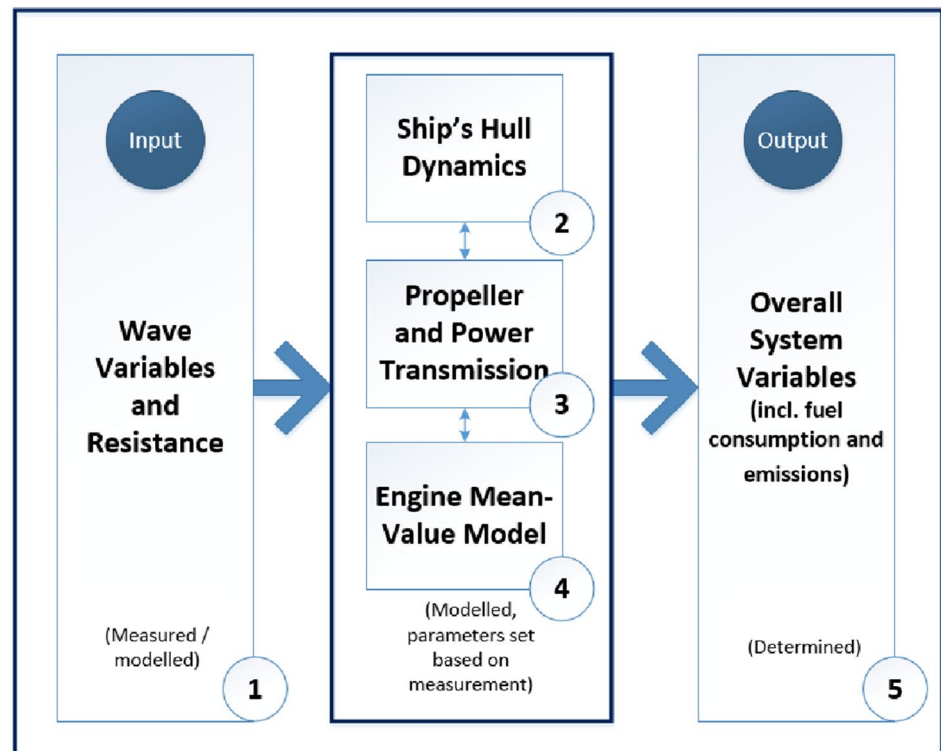
coupled equations of dynamics of ship motion, propeller, and engine, (2) total resistance that involves instantaneous wave forces in the x-direction (their mean value is known as added resistance), and (3) engine dynamics with the capability of determining the variables of the combustion process, and particularly combustion temperature. These subsystems are interacting with each other, and therefore, they had to be integrated under one overall system. To set up the model parameters, the steady-state data delivered by the manufacturers as well as some empirical relationships are used. Such a built model is then coded in MATLAB-SIMULINK. The simulation is conducted for a selected ship, in the calm water and head sea waves of two regular waves. Each subsystem of the model has been individually verified. Ship resistance, propeller characteristics, and wave variables are based on the model tests. The engine performances are verified for a wide range of steady-state conditions by simulating the engine variables when a selected operating point is changed from 100 to 10% of SMCR and vice versa. The increment of these changes was set from 10 to 50%.

Mathematical model

The layout of the mathematical model is presented in Fig. 1. It comprises five main modules, where the first (wave variables and resistance) and the fifth (overall system variables) modules stand as the input and output, respectively. Three other modules present the coupling equations of ship hull

dynamics, propeller performances, and engine unsteady-state variables.

Referring to Fig. 1, the first module has been already presented in [36]. The wave parameters were set in advance, and the variables of the generated wave are measured. It contains the calm water resistance and time series of wave force in the x-direction, which have been concluded from model tests. The second and third modules are described in [37]. The fourth module has been adapted so that the steady-state model applied in [36] is replaced by the mean-value zero-dimensional (MVZD) model described in [38]. The fifth module is elaborated to determine the overall system outputs, which integrates the outputs of modules 2, 3, and 4 by including their interrelations. A submodule for the NOx evaluation is developed and integrated under module 5, where the NOx formation model is evaluated based on the mathematical model presented in detail by Heywood [39]. The developed mathematical model enables determining the average NO emission directly, where NO_2 emission can be estimated roughly as 10% of the calculated NO emission [38]. The coupled system of equations representing the described mathematical model is shown in Table 1. The assumptions applied for these equations are: (1) all gases are semi-ideal, (2) the pressure and mass losses are negligible for all gases, (3) the mechanical losses are negligible, (4) the waves are regular, (5) the ship moves only along its longitudinal axes, when roll and pitch are omitted, and (6) ship is a rigid body.

Table 1 The mathematical model

Module 1	$R_{am}(t) = R_{tm}(t) - R_{Tm}(u(t))$	(1)
	$R_a(t) = \lambda^3 \cdot R_{am}(t)$	(2)
	$\omega_e = \omega\left(1 - u\frac{\omega}{g}\cos\mu\right)$	(3)
	$h(x, y, \mu, t) = \eta_3(t) + y \cdot \eta_4(t) - x \cdot \eta_5(t) - \zeta(x, y, \mu, t)$, where:	(4)
	$\eta_3(t) = \bar{\eta}_3 \cos\left(\omega_e t + \varphi_3\right)$	(5)
	$\eta_4(t) = \bar{\eta}_4 \cos\left(\omega_e t + \varphi_4\right)$	(6)
	$\eta_5(t) = \bar{\eta}_5 \cos\left(\omega_e t + \varphi_5\right)$	(7)
	$\zeta(x, y, \mu, t) = \bar{\zeta} \cos\left(kx\cos\mu + ky\sin\mu - \omega_e t\right)$	(8)
Module 2	$T_n(t) - R_T(u(t)) - R_a(t) = \left(\Delta + x_{\ddot{u}}\right)\dot{u}(t)$	(9)
Module 3	$J_A(t) = \dfrac{u_A(t)}{D_p\left|n_P(t)\right|}$	(10)
	$u_A(t) = u(t)(1 - w(t)) + \bar{u}_{PW}\cos\left(\omega_e t - kx_p\cos\mu\right)$, where: $w = 0.45\,C_p - 0.05(\text{Robertson})$	(11)
	$T(t) = \beta \cdot K_{T0}\left(J_A(t)\right)\rho n_P(t)\left|n_P(t)\right|D_P^4$, where $\beta = \text{real}\left(1 - \dfrac{\text{acos}\varepsilon}{\pi} + \dfrac{\varepsilon}{\pi}\sqrt{1 - \varepsilon^2}\right)$ and $\varepsilon = \dfrac{h}{R_P}$	(12)
	$Q_P(t) = K_Q\left(J_A(t)\right)\rho n_P(t)\left|n_P(t)\right|D_P^5$	(13)
	$T_n(t) = T(t)\left(1 - t_T(t)\right)$, where $t_T = 0.5C_p - 0.12(\text{Hecker})$	(14)
	$Q_E(t) - Q_P(t) = J\,\dot{\omega}(t)$	(15)
Module 4	Turbine:	
	$\dot{m}_5 = A_T^* \cdot \psi_T \cdot \sqrt{P_{gr} \cdot \rho_{gr}}$, where:	(16)
	$\psi_T\left(\pi_T\right) = \begin{cases} \left[\dfrac{2\kappa_T}{\kappa_T-1}\left(\pi_T^{\frac{2}{\kappa_T}} - \pi_T^{\frac{\kappa_T+1}{\kappa_T}}\right)\right]^{\frac{1}{2}}; \ \pi_T \geq \pi_{T_{cr.}} \\ \left[\kappa_T \cdot \left(\dfrac{2}{\kappa_T+1}\right)^{\frac{\kappa_T+1}{\kappa_T-1}}\right]^{\frac{1}{2}}; \qquad \pi_T < \pi_{T_{cr.}} \end{cases}$	(17)
	and	
	$\pi_{T_{cr.}} = \left(\dfrac{2}{\kappa_T+1}\right)^{\frac{\kappa_T}{\kappa_T-1}}$	(18)
	$P_T = \dot{m}_5 \cdot \eta_T \cdot \dfrac{\kappa_T}{\kappa_T-1} \cdot R_5 \cdot T_5 \cdot \left[1 - \pi_T^{\left(\frac{\kappa_T-1}{\kappa_T}\right)}\right]$	(19)
	Compressor:	
	$\dot{m}_1 = \dot{m}_1\left(\omega_{TC}, \pi_C, T_0\right)$; (compressor map)	(20)
	$P_C = \dfrac{1}{\eta_C} \cdot \dot{m}_1 \cdot \dfrac{\kappa_C}{\kappa_C-1} \cdot R_{at} \cdot T_{at} \cdot \left[1 - \pi_C^{\left(\frac{\kappa_C-1}{\kappa_C}\right)}\right]$	(21)
	$T_1 = \dfrac{1}{\eta_C} T_{at} \cdot \pi_C^{\frac{\kappa_T-1}{\kappa_T}}$	(22)
	Turbocharger shaft:	
	$\left(J_{TC}\dot{\omega}_{tc} = M_T - M_C - M_{TC_{loss}}\right)$	(23)
	Charge air cooler:	
	$T_2 = T_1 - \eta_{clr} \cdot \left(T_1 - T_w\right)$	(24)
	Intake air receiver:	
	$V_{am} \cdot \overset{\circ}{\rho}_{ia} = \dot{m}_1 - \dot{m}_3$	(25)

Table 1 (continued)

$$\frac{dT_{am}}{dt} = \frac{1}{m_{am}} \left[\left(\frac{c_{p2}}{c_{v_{am}}} \right) \cdot \dot{m}_2 \cdot T_2 - \left(\frac{c_{P_{am}}}{c_{v_{am}}} \right) \cdot \dot{m}_3 \cdot T_3 - T_{am} \cdot \dot{m}_{am} \right] \tag{26}$$

Exhaust gas receiver:

$$V_{gr} \cdot \overset{\circ}{\rho}_{gr} = \dot{m}_4 - \dot{m}_5 \tag{27}$$

$$\frac{dT_{gr}}{dt} = \frac{1}{m_{gr}} \left[\left(\frac{c_{p4}}{c_{v_{gr}}} \right) \cdot \dot{m}_4 \cdot T_4 - \left(\frac{c_{P_{gr}}}{c_{v_{gr}}} \right) \cdot \dot{m}_5 \cdot T_5 - T_{gr} \cdot \dot{m}_{gr} \right] \tag{28}$$

Engine cylinders and combustion process:

$$\dot{m}_3 = A_{cyl}^* \cdot \psi_{cyl}(\pi_{cyl}) \cdot \sqrt{p_3 \cdot \rho_3} \tag{29}$$

$$\dot{m}_{combt} = \frac{\omega}{2\pi} \cdot V_{cyl} \cdot \rho_3 \cdot Z \tag{30}$$

$$\eta_{fill} = 1 - \exp\left(-k_b \cdot \lambda_b\right), \text{where:} \lambda_b \approx \frac{\dot{m}_3}{\dot{m}_{combt}} \tag{31}$$

$$\dot{m}_{comb} = \frac{\omega}{2\pi} \cdot Z \cdot V_{cyl} \cdot \frac{R_{am}T_{am}}{p_{am}} \cdot \left[1 - \exp\left(-k_b \cdot \lambda_b\right)\right], \text{where:} \tag{32}$$

$$\lambda_b = \frac{2\pi \cdot \dot{m}_3 \cdot R_{am} \cdot T_{am}}{\omega \cdot Z \cdot V_{cyl}} \tag{33}$$

$$P_E = \eta_E \cdot \dot{m}_f \cdot q_f \tag{34}$$

$$T_4 = T_{am} \cdot \frac{c_{p3}}{c_{p4}} \cdot \frac{\dot{m}_3 - \dot{m}_{comb}}{\dot{m}_4} + T_{comb} \cdot \frac{\dot{m}_{comb}}{\dot{m}_4} \cdot \frac{c_{P_{comb}}}{c_{p4}} \tag{35}$$

$$T_{comb} = \frac{q_f \cdot \dot{m}_f \cdot (1 - k_{loss}) - P_E}{(\dot{m}_{comb} + \dot{m}_f) \cdot c_{p4}} + T_{am} \cdot \frac{\dot{m}_{comb}}{\dot{m}_{comb} + \dot{m}_f} \cdot \frac{c_{P_{am}}}{c_{p4}} \tag{36}$$

NOx emission

$$\frac{d[NO]}{dt} = \frac{6.10^{16}}{\sqrt{T_{comb}}} \exp\left(\frac{-69090}{T_{comb}} \right) [O_2]_e^{1/2} [N_2]_e \tag{37}$$

Results and discussion

In this section, the case study is presented, and the simulation process is described. Next, the results of the simulation are illustrated and interpreted. Finally, a detailed discussion is provided.

The selected ship is a container vessel, presented in [36], where the data regarding ship resistance and propeller parameters, as well as propulsive coefficients, are described based on the model tests, Zeraatgar and Ghaemi [37]. For clarification purposes, the ship and propeller specifications are given in Table 2. The engine is MAN-B&W 8S65ME-C8.5, equipped with a MAN B&W High Eff. TCA88 turbocharger [40, 41]. The fuel oil's low calorific value is assumed to equal 42,707 kJ/kg. The ambient conditions are 20 °C and 101,325 Pa. The kinematics of ship motion and the related coordination are set based on [42].

Ship motion and instantaneous wave force in the x-direction in two regular waves are recorded in towing tank in model scale of 40.75 as shown in Table 3.

Simulation is conducted for two considered waves as abbreviated W1 and W2 in Table 3. The simulation is continued in three more conditions, i.e., ship speed of 11.761, 10. 541 and 10.156 in the calm water. The results include the variables of the hull, propeller, and engine, including the internal variables of the engines. Additionally, fuel consumption and formation rate of NOx emission both in molar and mass terms are concluded and reported. The simulation time was set to 1800 s. The first 500 s are devoted to operation in the calm water, for the next approximately 800 s ship is in the wave, and finally, the last 500 s it is in the calm water.

When the ship is simulated for wave condition, based on the ship speed behaviour, it is concluded that the steady state has been approached approximately after 500 s. Therefore, the steady-state values of different variables could be selected for the time between 1200 and 1250, as the sample period. It should be noticed that the time during which the model in the experiment was in wave condition was not enough long to cover the whole simulation time. Therefore, the wave total force in the x-direction is repeated several times to cover 800 s for simulation purposes.

The variables that have been determined within the simulation process are about 43 (see Appendix). Some of the more important variables are depicted and discussed below.

The recorded resistance, as input, and the time traces of a set of selected variables are illustrated in Figs. 2, 3, 4, 5, 6, 7, 8, 9 and 10. Only those variables that play a fundamental role to demonstrate the NOx emission with respect to the ship operation conditions are selected, presented, and analysed.

Figure 2 depicts resistance fluctuation in two regular waves, W1 and W2, scaled up for ship from the model test [37]. The ship speed is 11. 7 m/s (22.8 Kn) and the calm water resistance is 1160.9 kN which its range of fluctuation is several times higher than the calm water resistance.

Figure 3 illustrates the time trends of ship speed. Starting from the calm water condition, the ship enters to head regular waves under the control strategy of constant engine speed. As a result, the ship speed reduces and fluctuates. Its mean value reaches 10.7 m/s and 10.2 m/s in W1 and W2, respectively. The fluctuation is not regular, and it repeats in each encounter period. Its amplitude is about 0.1 m/s and 0.15 m/s in W1 and W2, respectively. The ship speed reduction, however, could be more by excluding the governor, which tries to maintain the engine rotational speed at a constant level.

Figure 4 shows almost the same behaviour of engine rotational speed that was observed for ship speed due to the application of the same governor and its command signal. The mean value of the engine rotational speed changes from 9.72 to 9.82 and 9.80 RPM in W1 and W2, respectively. The amplitude of fluctuations is 1.0 RPM in W1 and 1.1 RPM in W2, which is not relatively too much. It is interesting to underline that the RPM fluctuation is a response to the resistance fluctuation in waves when the command rotational speed is kept at a constant level. Forcing the rotational speed to be maintained almost at a constant level means increasing the fuel consumption, and consequently higher emissions.

Figure 5 illustrates the fluctuation of propeller power demand. Its mean value is changed to 11,889 kW and 13,066 kW in W1 and W2, respectively. The propeller power demand amplitude is extremely high as much as ten times of the mean value where the higher wave height causes higher fluctuation amplitude.

Table 3 Parameters of the generated regular waves for the model tests [37]

No	H		T	
	Model (cm)	Ship (m)	Model (s)	Ship (s)
W1	4	1.63	1.13	7.23
W2	8	3.26	1.60	10.21

Figure 6 demonstrates the engine delivered power. It is achieved under circumstances of constant engine speed strategy as well as engine limiters. Its mean value in the calm water is 19319 kW and reduces to 10,908 kW and 11,240 kW in W1 and W2, respectively. It is extremely high and is in impact form fluctuating as time marches. It should be noted that this is mostly related to the control strategy, as well as the diesel engine characteristics.

Figure 7 shows the spatial average of the temperature of combustion as a function of time. It follows the same trend as engine-delivered power following the constant rotational speed control strategy. Considering that the NOx emission is strongly dependent on this temperature, it changes in a vast range and very large fluctuations of the emissions should be expected in waves.

Fuel rate and consumed fuel are shown in Fig. 8. The mean fuel rate changes from 0.879 kg/s to 0.536 kg/s and 0.561 kg/s in W1 and W2, respectively. To avoid any confusion, the fuel rate at a ship speed of 10.561 m/s and 10.156 m/s in the calm water condition (equivalent to the mean ship speed at W1 and W2) is calculated and shown in Table 4. They are 0.570 kg/s and 0.536 kg/s, respectively. It is well known that the ship power is a function of power 3 to 4 of ship speed, while fuel rate is in the proportion of ship power. That is why a marginal change in the mean value of ship speed results in a significant change in the fuel rate.

The values of the consumed fuel in W1 and W2 are marginally different. Again, it is mainly related to the selected control strategy, which keeps the rotational speed at a constant level independent of the external and environmental conditions.

To show the impact of wave parameters, hull, propeller, and engine dynamics in sea waves on the NOx formation, the mean values of the variables presented in Figs. 2, 4, 5,

Table 2 Ship and propeller specifications [36, 37]

Ship	Δ (ton)	L_{BP} (m)	B (m)	T (m)	u (m/s)	C_B (–)	C_P (–)
	26,980.22	182.880	24.414	9.782	23.82	0.600	0.615
Propeller		D_P (m)		Z_P (–)		A_E/A_0 (–)	H/D_P (–)
		7.590		5		0.5808	1.00

Fig. 2 Total resistance fluctuations for two wave conditions (upper part: overall, lower part: during the selected period in steady state)
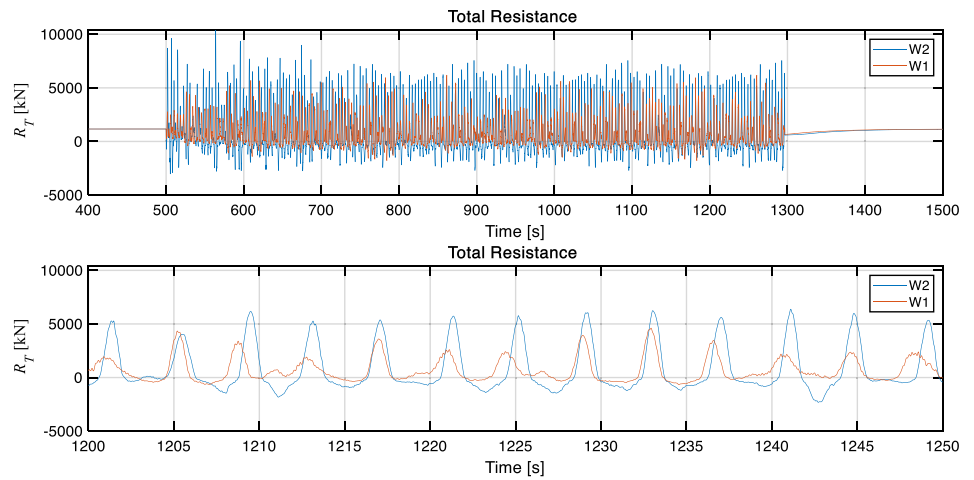

Fig. 3 Ship speed versus time for two wave conditions (upper part: overall, lower part: during the selected period in steady state)
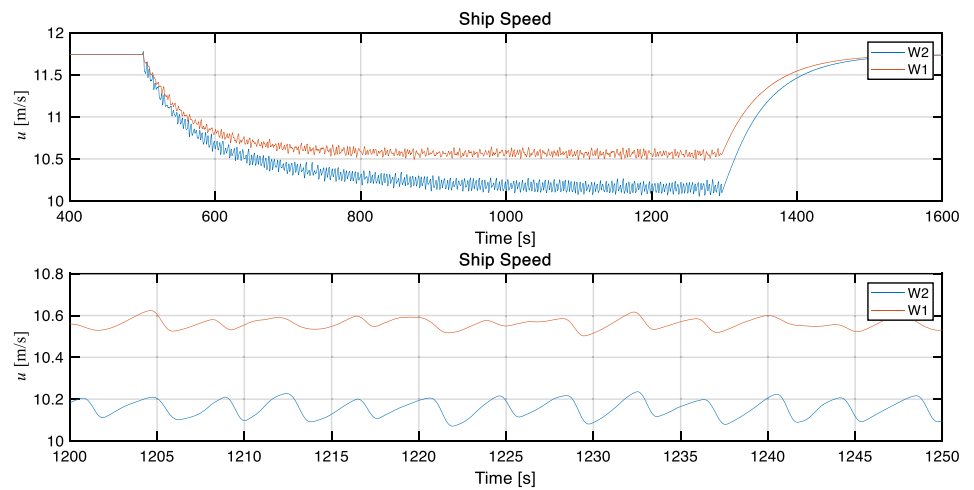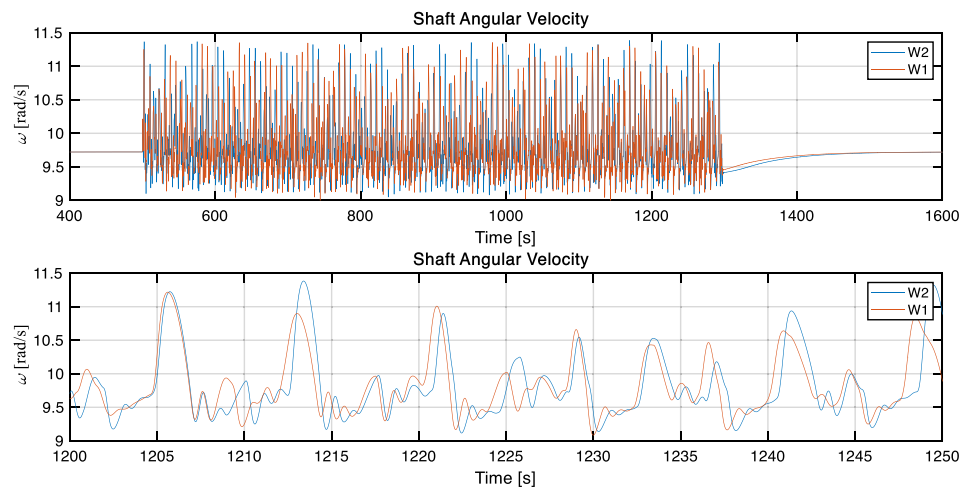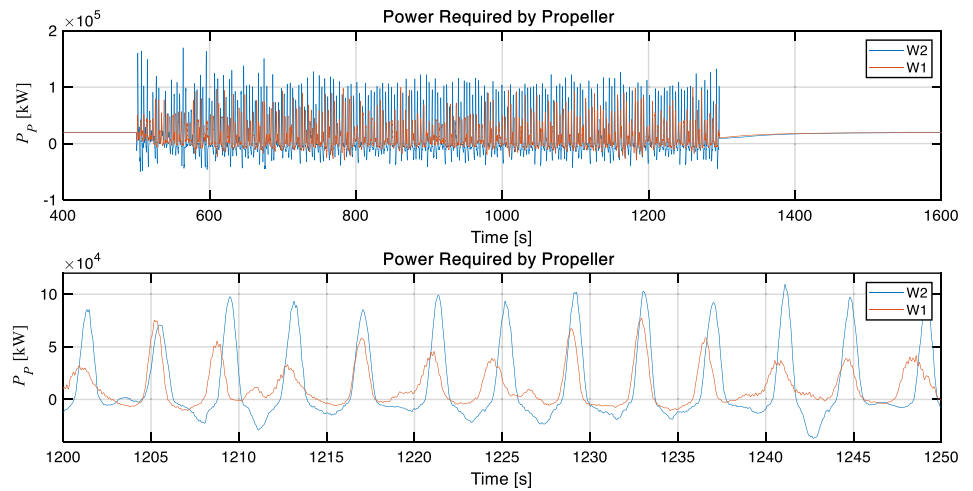

Fig. 4 Engine speed versus time for two wave conditions (upper part: overall, lower part: during the selected period in steady state)


6, 7, 8, 9 and 10 are evaluated and given in Table 4. Since the comparison to the calm water condition is necessary, the selected variables are calculated for three ship speeds: (1)

$u = 11.741$ m/s, and no wave, (2) $u = 10.561$ m/s, equivalent to the ship mean speed in W1 navigating in the calm water, and (3) $u = 10.156$ m/s, equivalent to ship mean speed in

Fig. 5 Propeller power demand versus time for two wave conditions (upper part: overall, lower part: during the selected period in steady state)

Fig. 6 Engine delivered power versus time for two wave conditions (upper part: overall, lower part: during the selected period in steady state)
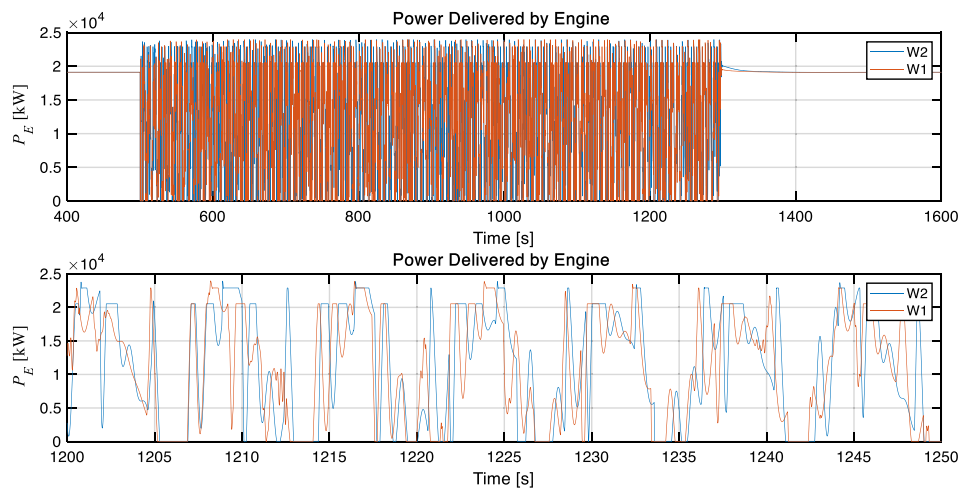
Fig. 7 Average combustion temperature versus time for two wave conditions (upper part: overall, lower part: during the selected period in steady state)
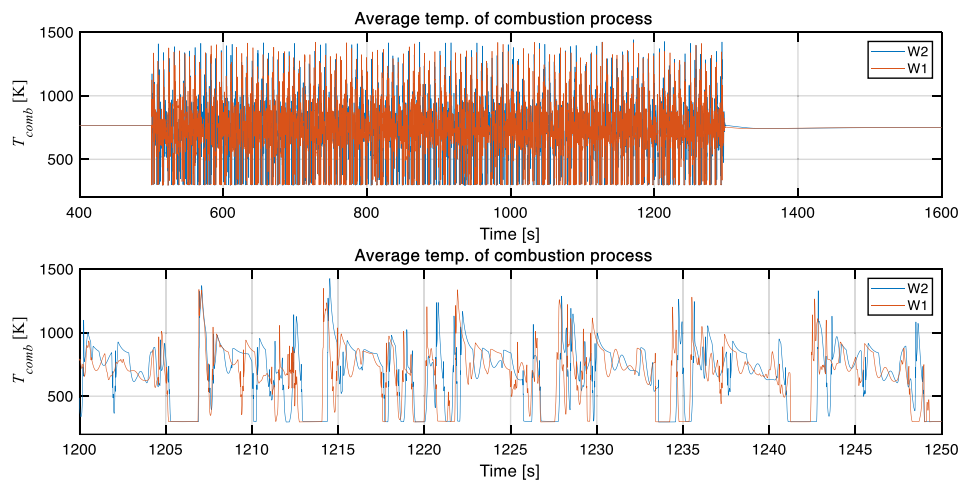
W2 navigating in the calm water. The mean value of the variables under the wave condition is calculated for the selected period of 50 s (from 1200 to 1250 s), where the ship is assumed to be in steady repeating oscillation.

Hereafter, the discussion is provided. Referring to the system of Eqs. (1) to (37) total resistance and fuel rate controlled by the speed governor are dominating inputs that decide the time trend of other variables. As it is shown in

Fig. 8 Fuel rate (upper part) and consumed fuel (lower part) versus time for two wave conditions
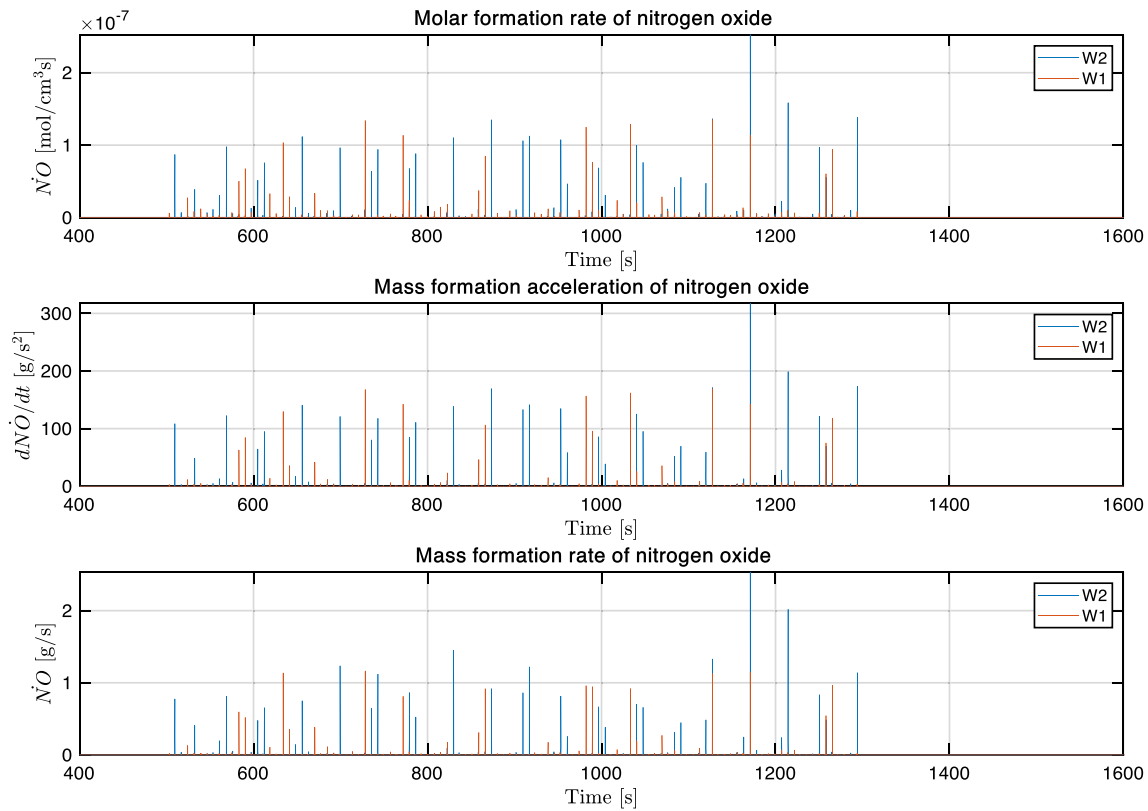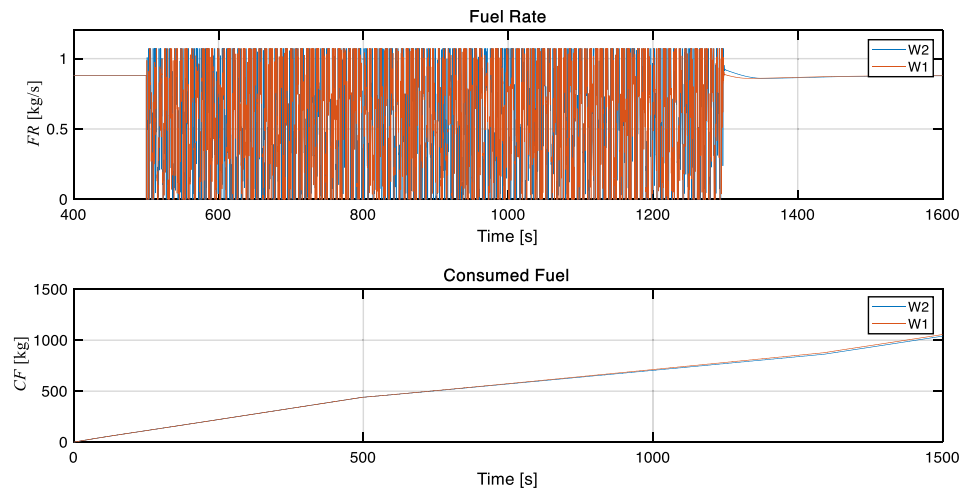
Fig. 9 Formation of NO: molar formation rate (upper part), mass formation acceleration (middle part), and mass formation rate (lower part) versus time for two wave conditions

Fig. 2, the fluctuations of the total resistance due to the encountered wave are quite large. It becomes negative in some instances along a period, which means the ship is pushed forward by the sea wave despite the head sea condition. The negative values of total resistance are observed when the ship encounters the wave trough, depending on the wavelength to ship length ratio. However, the magnitude

of the total resistance in such a condition is much less than the magnitude of the total resistance at the maximum level. Referring to the results given in Table 4, the added resistance in W1 and W2 is approximately 52 kN and 176 kN, respectively. However, the min and max values of total resistance are −670 kN and +4609 kN in W1, and −2315 kN and +6380 kN in W2. The impact of resistance fluctuations
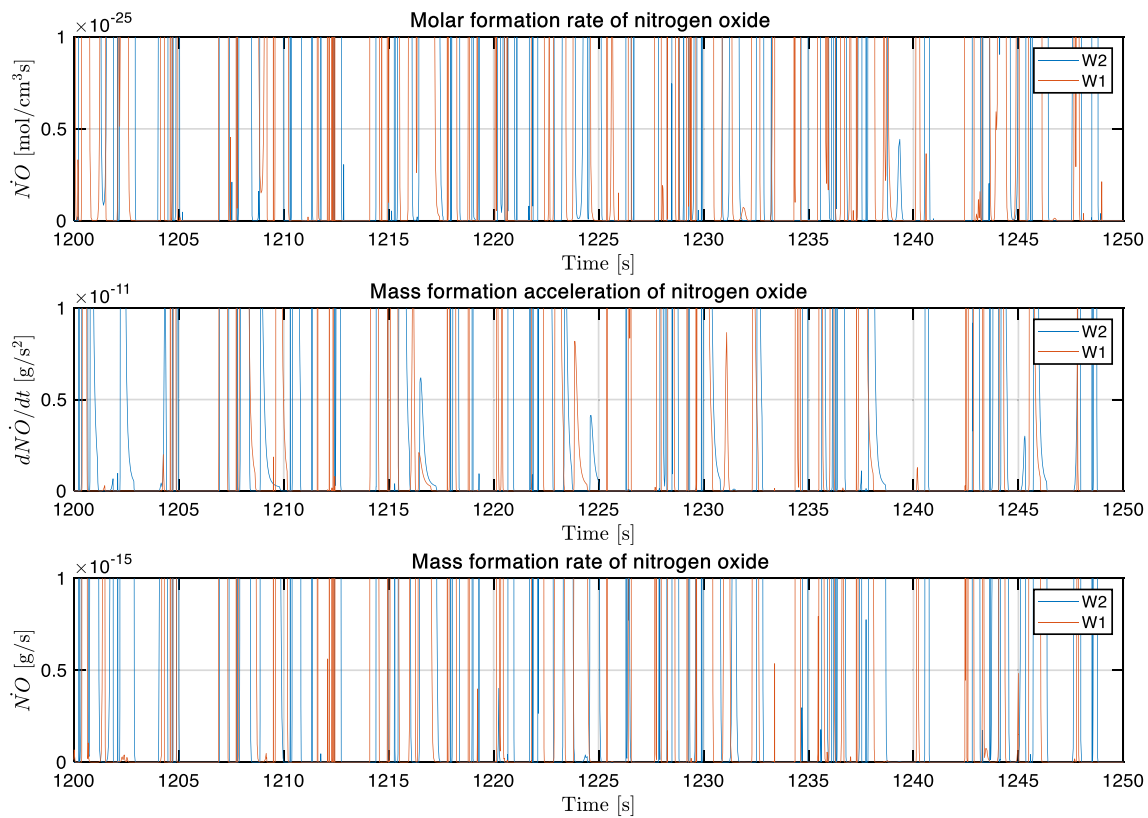
Fig. 10 A selected period in a steady state of formation of NO or NOx: molar formation rate (upper part), mass formation acceleration (middle part), and mass formation rate (lower part) for two wave conditions

Table 4 Mean values of the selected variables of the system

Variable	Unit	Calm ($u = 11.741$ m/s)	Calm ($u = 10.561$ m/s)	Calm ($u = 10.156$ m/s)	W1	W2
Total resistance	kN	1160,889	660,272	599,131	712,436	775,719
Ship speed	m/s	11,741	10,561	10,156	10,561	10,156
Engine rotational speed	rad/s	9721	9723	9828	9824	9804
Required power by propeller	kW	19,301	6706	6085	11,889	13,066
Delivered power by engine	kW	19,319	6710	6089	10,908	11,240
Average combustion temperature	K	767	695	691	689	702
Voyaged distance	m	587.049	528.050	507.800	528.055	507.798
Fuel rate	kg/s	0.879	0.570	0.536	0.536	0.561
Consumed fuel	kg	43.928	28.489	26.826	26.823	28.074
Consumed fuel per metre	kg/m	0.075	0.054	0.053	0.051	0.055
Molar formation of nitrogen oxide	mol/m3.s	1.731E−25	1.71E−29	9.060E−30	2.334E−11	1.689E−10
Mass formation acceleration of nitrogen oxide	g/s^2	1.895E−16	1.38E−20	6.926E−21	2.212E−02	2.065E−01
The mass formation rate of nitrogen oxide	g/s	6.377E−17	6.915E−19	3.463E−19	1.914E−04	2.131E−03
Emitted nitrogen oxide	kg	9.630E−18	3.96E−16	1.98E−16	4.967E−04	5.566E−04
Specific emitted nitrogen oxide	g/kWh	1.188E−17	3.710E−19	2.048E−19	6.317E−05	6.825E−04

in a large range of variation on the rate of formation of NOx can be observed in Figs. 9 and 10. The NOx itself is the result of the frequent and large variation of average combustion temperature shown in Fig. 7., which represents approximately 1200 °C oscillations, periodically. The latter has a direct influence on NOx emission, which is described by Eq. (37). The relationship between combustion temperature and molar formation rate of NO is shown in Fig. 11. It illustrates how temperatures higher than 1211 °C lead to molar formation rates of NO beyond 1E−6 mol/cm³s. It can be regarded as a limit that causes higher NOx emission than 1 to 2 g/kWh (the lower bound of IMO Tier III is 1.96 g/kWh) for the considered case depending on the mass flow rate to the engine cylinders.

It should be also noted that the combustion temperature considered in this study is an average value that is calculated based on the MVZD model of the engine. It means that the combustion continuously happens in time but at a lower temperature. The instantaneous value in comparison with the mean value of this temperature during the combustion process is several times higher, and consequently, the instantaneous emission rate is significantly higher, too. Therefore, the results are generally underestimated and must be regarded as conservative just for comparative analysis. However, the simulation results in the calm water, W1, and W2 conditions, relatively well describe the sea waves' impact on the NOx emissions. In other words, the MVZD model can help to compare the impact of ship environment on the NOx emission but is not able to provide a real and exact figure for NOx formation rate. The present study can be further developed to adopt IVZD or IVMD as an engine model to improve the NOx emission determination.

As an example, the mass formation rate of NO, given in Table 4, of 6915E−19 and 3463E−19 in calm water jumps up to 1914E−04 and 2131E−03 in W1 and W2 conditions, respectively. Even though the mean value of averaged combustion temperature changes in a small range. That is due to large fluctuations of the NO formation rate shown in Fig. 9. These radical, large, and frequent fluctuations are the results of the applied control strategy, which is based on using a conventional governor to keep the engine rotational speed at a constant level. Such a strategy leads to a quick response to the environmental disturbances and significant change in the fuel rate in wave conditions, see Fig. 8. It is also the reason for the rapid fluctuations of the engine power as shown in Fig. 6. To summarize, based on the given values in the last row of Table 4, it is determined that emitted nitrogen oxide in terms of kg/kWh has been increased approximately 1.7E14 times more in the W1 condition and 3.3E15 times in the W2 condition, compared to their related calm water conditions, i.e. for ship speeds 10.561 m/s and 10.156 m/s, respectively. This addresses the need of changing the control
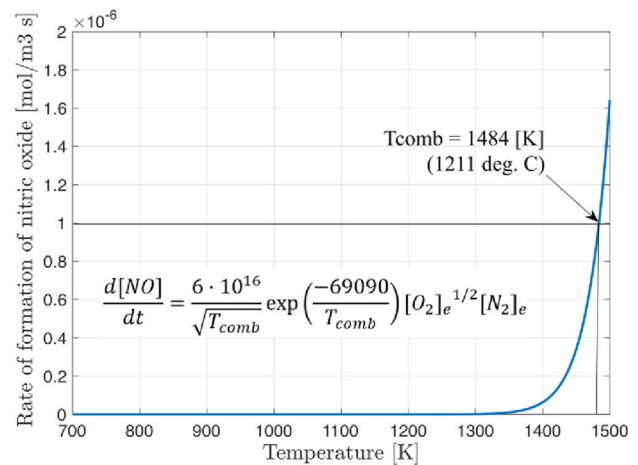

Fig. 11 The rate of formation of nitrogen dioxide as a function of combustion temperature

$$\frac{d[NO]}{dt} = \frac{6 \cdot 10^{16}}{\sqrt{T_{comb}}} \exp\left(\frac{-69090}{T_{comb}}\right) [O_2]_e^{1/2} [N_2]_e$$

strategy to decrease the emissions in wave conditions, which of course should be adjusted with no safety sacrificing.

Conclusions

The present study aims to investigate the influence of sea waves on the NOx emission of a selected ship equipped with a conventional marine diesel engine that is controlled by a governor to keep the engine and propeller rotational speed at a constant level. For this purpose, a proper mathematical model is developed in which the hull, propeller, and engine interactions are taken into consideration. The model is then adapted for numerical simulation. The parameters of the model have been set based on the experimental tests or manufacturers' data. To do the comparative analysis, the simulation is conducted in two regular waves and three ship speeds in the calm water condition. There are five main findings of this study. Firstly, it is concluded that sea waves have a significant impact on the emitted NOx in comparison with the calm water condition at the same ship speed. Secondly, the simulation results show that the higher wave height causes higher total resistance in waves and in turn the emitted NOx becomes higher. The third one describes the reason for the radical increase of NOx in waves. It indicates that such a significant increase is associated with the conventional control strategy that is based on constant engine rotational speed using a conventional speed governor, which is a usual practice in ship navigation. Following this finding, the fourth one can be formulated. The traditional control strategy of the constant engine rotational speed rapidly changes the instantaneous fuel rate to compensate the influence of instantaneous wave added resistance. This leads to the high variation

Table 5 The list of output variables of the computer code

1. Ship speed
2. Engine speed
3. Advance number
4. Propeller thrust and torque diminution factor
5. Net thrust
6. Propeller torque
7. Engine torque
8. Required brake power
9. Delivered brake power
10. Mass of air in the air manifold
11. Temp. of air in the air manifold
12. Mass of ex. gases in the ex. gases receiver
13. Temp. of ex. gases in the ex. gases receiver
14. The mass flow rate of exhaust gases after the turbine
15. Temp. of ex. gases after turbine
16. Average temp. of combustion process
17. Average temp. of outflow gases from engine cylinders
18. Fuel rate
19. The flow rate of air after the compressor
20. The flow rate of air into cylinders
21. The flow rate of air that takes part in combustion
22. The flow rate of exhaust gases after cylinders
23. The flow rate of exhaust gases into the turbine
24. The temperature of the air after the compressor
25. The temperature of air into cylinders
26. The temperature of air that takes part in combustion
27. The temperature of exhaust gases into turbine
28. The temperature of exhaust gases after the turbine
29. The pressure ratio of the compressor
30. The pressure ratio of the turbine
31. The tip speed of the compressor wheel
32. Power of compressor
33. Power of turbine
34. Angular velocity of the turbocharger shaft
35. Mass of air in the intake air manifold
36. The temperature of the air in the intake air manifold
37. The pressure of air in the intake air manifold
38. Mass of gases in exhaust gas receiver
39. The temperature of gases in the exhaust gas receiver
40. The pressure of gases in the exhaust gas receiver
41. Angular velocity of the engine shaft
42. Fuel-to-air ratio
43. The formation rate of nitrogen oxide

in temperature of gases in the combustion process which is blamed for the radical increase of emitted NOx. Summing up these four findings and the extent of the impact of sea wave conditions on the emissions in waves puts under question employing the traditional control strategy of constant engine rotational speed, and this is the final finding and overall conclusion of the study. It underlines that an alternate control strategy is necessary which avoids high and radical changes in fuel rate, prevents sharp and frequent change in combustion temperature and tremendously improves the emission performance of the engine. In addition to this future research need, adequate control of the air mass flow into the engine that leads to reduction of NOx emission should be carefully studied. Further investigations should be accompanied by employing an IVZD or IVMD model of the engine for stimulation purposes since the MVZD model is suitable for comparative analysis of NOx emission rather than determining its absolute values.

Appendix 1

The variables that are determined as the outputs of the simulation code are given in Table 5.

Declarations

References

1. Vasilescu, M.V.: Advantages and disadvantages of different types of modern marine propulsions. J. Mar. Technol. Environ. **2**, 57–63 (2018)

2. Reşitoğlu, İA., Altinişik, K., Keskin, A.: The pollutant emissions from diesel-engine vehicles and exhaust aftertreatment systems. Clean Tech. Environ. Policy **17**, 15–27 (2015). https://doi.org/10.1007/s10098-014-0793-9

3. Lawrence, M.G., Crutzen, P.J.: Influence of NO(x) emissions from ships on tropospheric photochemistry and climate. Nature **402**(6758), 167–170 (1999). https://doi.org/10.1038/46013

4. Contini, D., Merico, E.: Recent advances in studying air quality and health effects of shipping emissions. Atmosphere **12**(1), 92 (2021). https://doi.org/10.3390/ATMOS12010092

5. Joung, T.H., Kang, S.G., Lee, J.K., Ahn, J.: The IMO initial strategy for reducing Greenhouse Gas(GHG) emissions, and its follow-up actions towards 2050. J. Int. Mar. Saf. Environ. Aff. Shipp. **4**(1), 1–7 (2020). https://doi.org/10.1080/25725084.2019.1707938

6. Bouman, E.A., Lindstad, E., Rialland, A.I., Stromman, A.H.: State-of-the-art technologies, measures, and potential for reducing GHG emissions from shipping – a review. Transp. Res. Part D Transp. Environ. **52**, 408–421 (2017). https://doi.org/10.1016/j.trd.2017.03.022

7. Lamas, M.I., Rodriguez, C.G.: Emissions from marine engines and NOx reduction methods. J. Marit. Res. **9**, 77–81 (2012)

8. Park, W., Lee, J., Min, K., Yu, J., Park, S., Cho, S.: Prediction of real-time NO based on the in-cylinder pressure in Diesel engines. Proc. Combust. Inst. **34**(2), 3075–3082 (2013). https://doi.org/10.1016/j.proci.2012.06.170

9. Lu, X., Geng, P., Chen, Y.: NOx emission reduction technology for marine engine based on tier-III: a review. J. Therm. Sci. **29**(5), 1242–1268 (2020). https://doi.org/10.1007/S11630-020-1342-Y

10. Liang, X.Y., Zhou, P.L., Yu, H.Z.N., Cao, X.Y., Sun, X.X.P.L.: Computational study of NOx reduction on a marine diesel engine by application of different technologies. Energy Procedia **158**, 4447–4452 (2019)

11. Deng, J., Wang, X., Wei, Z., Wang, L., Wang, C., Chen, Z.: A review of NOx and SOx emission reduction technologies for marine diesel engines and the potential evaluation of liquefied natural gas fuelled vessels. Sci. Total Environ **766**, 144319 (2021)

12. Jeevahan, J., Mageshwaran, G., Britto, J.G., Durai Raj, R.B., Thamarai, K.R.: Various strategies for reducing NOx emissions of biodiesel fuel used in conventional diesel engines: a review. Chem. Eng. Commun. **204**(10), 1202–1223 (2017). https://doi.org/10.1080/00986445.2017.1353500

13. Cakir, H.: Nitric oxide formation in diesel engines. Inst. Mech. Eng. (Lond) Proc. **188**(46), 477–483 (1974). https://doi.org/10.1243/PIME_PROC_1974_188_057_02]

14. Way, R.J.B.: Methods for determination of composition and thermodynamic properties of combustion products for internal combustion engine calculations. Inst. Mech. Eng. Lond. Proc. **190**(60), 686–697 (1976). https://doi.org/10.1243/PIME_PROC_1976_190_073_02

15. Miller, J.A., Bowman, C.T.: Mechanism and modelling of nitrogen chemistry in combustion. Prog. Energy Combust. Sci. **15**(4), 287–338 (1989). https://doi.org/10.1016/0360-1285(89)90017-8

16. Correa, S.M.: A review of NOx formation under gas-turbine combustion conditions. Combust. Sci. Technol. **87**(1–6), 329–362 (1993). https://doi.org/10.1080/00102209208947221

17. Chikahisa, T., Konno, M., Murayama, T., Kumagai, T.: Analysis of NO formation characteristics and its control concepts in diesel engines from NO reaction kinetics. JSAE Rev. **15**(4), 297–303 (1994). https://doi.org/10.1016/0389-4304(94)90210-0

18. Kikuta, K., Chikahisa, T., Hishinuma, Y.: Study on predicting combustion and NOx formation in diesel engines from scale model experiments. JSME Int. J. Ser. B **43**(1), 89–96 (2000). https://doi.org/10.1299/JSMEB.43.89

19. Rausen, D.J., Stefanopoulou, A.G., Kang, J.M., Eng, J.A., Kuo, T.W.: A mean-value model for control of homogeneous charge compression ignition (HCCI) engines. J. Dyn. Syst. Meas. Control Trans. ASME **127**(3), 355–362 (2005). https://doi.org/10.1115/1.1985439

20. Merker, G.P.: Simulating Combustion: Simulation of Combustion and Pollutant Formation for Engine-Development. Springer, New York (2006)

21. Asprion, J., Chinellato, O., Guzzella, L.: A fast and accurate physics-based model for the NOx emissions of diesel engines. Appl. Energy **103**, 221–233 (2013). https://doi.org/10.1016/J.APENERGY.2012.09.038

22. Arregle, J., Lopez, J.J., Guardiola, C., Monin, C.: Sensitivity Study of a NOx Estimation Model for On-board Applications. SAE Technical Papers, SAE International (2008). https://doi.org/10.4271/2008-01-0640

23. Egnell, R.: Combustion Diagnostics by Means of Multizone Heat Release Analysis and NO Calculation. SAE Technical Papers, SAE International (1998). https://doi.org/10.4271/981424

24. Lamaris, V.T., Hountalas, D.T., Zannis, T.C., Glaros, S.E.: Development and validation of a multi-zone combustion model for predicting performance characteristics and NOx emissions in large scale two-stroke diesel engines. ASME Int. Mech. Eng. Congr. Expo. Proc. **3**, 317–327 (2010). https://doi.org/10.1115/IMECE2009-11382

25. Mocerino, L., Soares, C.G., Rizzuto, E., Balsamo, F., Quaranta, F.: Validation of an emission model for a marine diesel engine with data from sea operations. J. Mar. Sci. Appl. (2021). https://doi.org/10.1007/S11804-021-00227-W/FIGURES/13

26. Papagiannakis, R.G., Rakopoulos, C.D., Hountalas, D.T., Rakopoulos, D.C.: Emission characteristics of high speed, dual fuel, compression ignition engine operating in a wide range of natural gas/diesel fuel proportions. Fuel **89**(7), 1397–1406 (2010). https://doi.org/10.1016/J.FUEL.2009.11.001

27. Benvenuto, G., Laviola, M., Campora, U.: Simulation Model of a Methane-Fuelled Four Stroke Marine Engine for Studies on Low Emission Propulsion Systems. Developments in Maritime Transportation and Exploitation of Sea Resources, pp. 591–598. CRC Press, Florida (2013)

28. Stoumpos, S., Theotokatos, G., Boulougouris, E., Vassalos, D., Lazakis, I., Livanos, G.: Marine dual fuel engine modelling and parametric investigation of engine settings effect on performance-emissions trade-offs. Ocean Eng. **157**, 376–386 (2017). https://doi.org/10.1016/J.OCEANENG.2018.03.059

29. Scappin, F., Stefansson, S.H., Haglind, F., Andreasen, A., Larsen, U.: Validation of a zero-dimensional model for prediction of NOx and engine performance for electronically controlled marine two-stroke diesel engines. Appl. Therm. Eng. **37**, 344–352 (2012). https://doi.org/10.1016/J.APPLTHERMALENG.2011.11.047

30. Hountalas, D.T., Zovanos, G.N., Sakellarakis, D., Antonopoulos A.K.: Validation of multi-zone combustion model ability to predict two stroke diesel engine performance and NOx emissions using on board measurements. In: Proceedings of the Spring Technical Conference of the ASME Internal Combustion Engine Division, pp. 47—60 (2012). https://doi.org/10.1115/ICES2012-81100

31. Savva, N.S., Hountalas, D.T.: Evolution and application of a pseudo-multi-zone model for the prediction of NOx emissions from large-scale diesel engines at various operating conditions. Energy Convers. Manag. **85**, 373–388 (2014). https://doi.org/10.1016/j.enconman.2014.05.103

32. Raptotasios, S.I., Sakellaridis, N.F., Papagiannakis, R.G., Hountalas, D.T.: Application of a multi-zone combustion model to

investigate the NOx reduction potential of two-stroke marine diesel engines using EGR. Appl. Energy **157**, 814–823 (2015). https://doi.org/10.1016/J.APENERGY.2014.12.041

33. Larsen, U., Pierobon, L., Baldi, F., Haglind, F., Ivarsson, A.: Development of a model for the prediction of the fuel consumption and nitrogen oxides emission trade-off for large ships. Energy **80**, 545–555 (2015). https://doi.org/10.1016/J.ENERGY.2014.12.009

34. Cooper, D.A.: Exhaust emissions from high-speed passenger ferries. Atmos Environ. (2001). https://doi.org/10.1016/s1352-2310(01)00192-3

35. Kowalski, J., Tarelko, W.: NOx emission from a two-stroke ship engine Part 1: modeling aspect. Appl. Therm. Eng. **29**(11–12), 2153–2159 (2009). https://doi.org/10.1016/j.applthermaleng.2008.06.032

36. Zeraatgar, H., Ghaemi, M.H.: The analysis of overall ship fuel consumption in acceleration manoeuvre using hull-propeller-engine interaction principles and governor features. Pol. Marit. Res. **26**, 162–173 (2019). https://doi.org/10.2478/pomr-2019-0018

37. Ghaemi, M., Zeraatgar, H.: Analysis of hull, propeller and engine interactions in regular waves by a combination of experiment and simulation. J. Mar. Sci. Technol. (2020). https://doi.org/10.1007/s00773-020-00734-5

38. Ghaemi, M.H.: Performance and emission modelling and simulation of marine diesel engines using publicly available engine data. Pol. Marit. Res. **28**(4), 63–87 (2021). https://doi.org/10.2478/POMR-2021-0050

39. Heywood, J.: Internal Combustion Engine Fundamentals. McGraw-Hill Education Ltd, New York (2018)

40. MAN-B&W: Computerized Engine Application System (CEAS). https://www.man-es.com/marine/products/planning-tools-and-downloads/ceas-engine-calculations. Accessed 05 Apr 2022

41. MAN B&W S65ME-C8.5-TII Project Guide Electronically Controlled Two-stroke Engines, https://www.academia.edu/35674638/MAN_B_and_W_S90ME_C8_TII_Project_Guide_Electronically_Controlled_Two_stroke_Engine. Accessed 03 Apr 2022

42. Fossen, T.I.: Handbook of marine craft hydrodynamics and motion control [bookshelf]. IEEE Control Syst. **36**, 78–79 (2016). https://doi.org/10.1109/mcs.2015.2495095

Publisher's Note Springer Nature remains neutral with regard to jurisdictional claims in published maps and institutional affiliations.